IEEE Access
Multidisciplinary ⋮ Rapid Review ⋮ Open Access Journal

Received January 31, 2020, accepted February 5, 2020, date of publication February 10, 2020, date of current version February 18, 2020.

Digital Object Identifier 10.1109/ACCESS.2020.2972973

A New Illumination-Rotation-Invariance Texture Feature Based on Quasi-Periodic Signal Analysis

ZHIHUA YANG[1], QIAN ZHANG[2], AND FENG ZHOU[1]
[1]Information Science School, Guangdong University of Finance and Economics, Guangzhou 510320, China
[2]Mathematics and Statistics, Shenzhen University, Shenzhen 518060, China

Corresponding author: Qian Zhang (mazhangq@szu.edu.cn)

This work was supported in part by the National Natural Science Foundation of China under Grant 11601346 and Grant 11901113, and in part by the Guangzhou Science and Technology Plan Project under Grant 201904010225.

ABSTRACT Texture classification is a classic problem in pattern recognition. It is an effective strategy for improving texture classification to find the texture features with both powerful discrimination and various invariant properties. In this paper, we provide a new insight into texture images, that is, texture images can be treated as quasi-periodic signals. Some new concepts such as Dominant Period Component (DPC), periodic degree (PD), and Main Frequency (MF) are proposed to characterize the properties of quasi-periodic signals. DPC controls the oscillation rate of a quasi-periodic signal and plays a key role in controlling the behavior of the whole signal. So it can serve as a key feature for texture classification. Based on this idea, we propose a new method to extract texture features. The proposed features have both powerful classification ability and rotation-illumination- invariance as well as robustness to noise. Experimental results on three texture data sets demonstrate the validity of this method.

INDEX TERMS Quasi-periodic signal, main-frequency, texture feature, Hilbert marginal spectrum.

I. INTRODUCTION

Texture is a special kind of image. Texture images are composed of some basic elements that are similar to each other and interlaced with each other. Texture classification is a classical problem in pattern recognition. Its applications include remote sensing image analysis and understanding, automatic recognition of organs in medical images, content-based image retrieval to text page segmentation and so on.

Texture classification is a very difficult problem, since a good texture classification method needs having not only strong classification ability, but also scale-, rotation-, illumination- and other invariant properties, as well as robustness to noise. Therefore, texture classification has always been a challenging topic in the field of pattern recognition. Many texture classification methods have been proposed [1]–[9].

One of the most important strategies of texture classification is to find such features that have both powerful discrimination and some invariant properties, such as rotation- [10], [11], scale- [12]–[14] and illumination-invariance [15], [16], as well as the robustness to noise [17]. Some new techniques such as graph signal processing and machine learning have also been introduced to produce features with various invariant properties [18], [19].

Inspired by the current works, we try to view the texture image from a new perspective, that is, treating the texture images as quasi-periodic signals.

Quasi-periodic signals widely exist in the real world. The studies on them can be traced back to as early as 1932 [20]. A signal is said to be quasi-periodic when it shows periodicity to some extent, but does not strictly meet the definition of periodic signals [21]. Generally, a quasi-periodic signal can be regarded as a linear superposition of some periodic components whose periods have no least common multiples. Extracting harmonic components by using various filters is the classic processing of analyzing quasi-periodic signals [22]–[24].

However, as well known, quasi-periodic signals are typically non-stationary, which implies that the harmonic components extracted by using the filters could not be their intrinsic characterization. The reason is that most of the filters themself are designed based on the Fourier transform or its deformations.

We realize that the dominant periodic behavior of a quasi-periodic signal is actually controlled by the component which

The associate editor coordinating the review of this manuscript and approving it for publication was Lefei Zhang.

possesses the largest energy. For the sake of simplicity, we refer the component as Dominant Period Component (DPC). However, how do we pick out the DPC from a real quasi-periodic signal? How to evaluate its capability to control the whole signal's periodic behavior? In this manuscript, a fully data-driven algorithm, namely the Empirical Mode Decomposition (EMD) [25] is firstly employed to adaptively decompose a quasi-periodic signal into some Intrinsic Mode Functions (IMFs). According to the work of Flandrin et al., EMD essentially acts as an adaptive filter bank [26]. Therefore, the IMFs can be regarded as the substitutes of the harmonic components in the Fourier transform, but are more natural than them. In the literature [25], the energy distribution of IMFs on the time-frequency plane is defined as Hilbert spectrum, from which the so-called marginal spectrum could also be obtained easily, which is an energy distribution of a signal along the frequency axis. It will be shown that the frequency corresponding to DPC of a quasi-periodic signal may be easily detected from its marginal spectrum. As we have known, the frequency controls the signal's oscillation rate and thus is an important property of a periodic signal. Similarly, for a quasi-periodic signal, its DPC's frequency also should play a key role to control the whole signal's periodic behavior. When it is used as a feature to discriminate different quasi-periodic signals, a good performance will be worth expecting.

Since the texture images can be regarded as quasi-periodic signals, the above analysis method is naturally suitable for the analysis of texture images. This inspires us to think deeply such a problem that whether can we find effective texture features based on the quasi-periodic signal analysis of texture images? Based on the idea, we propose a new texture classification feature with illumination-rotation-invariant properties and give the theoretic explanation. Experimental results demonstrate the validity of the proposed feature.

The main contributions of this manuscript include that 1) Firstly introduce the concepts of Dominant Period Component (DPC), periodic degree (PD), and Main Frequency (MF); 2) Properties of MF and PD are concluded; 3) EMD as well as Hilbert-Huang Transform are introduced to analysis quasi-periodic signals; 4) Propose a novel texture classification feature.

The following sections of this manuscript are organized as follows. In Section 2, the concepts of main frequency and periodic degree of a quasi-periodic signal are given and some related properties are discussed. In Section 3, we introduce a new method of extracting features from a texture image, and the rotation-illumination-invariant properties as well as the robustness to noise are discussed. Section 4 presents some experiments, and the concluding remarks are made in Section 5.

II. MAIN FREQUENCY OF A QUASI-PERIODIC SIGNAL

Consider the following signal

$$x(t) = x_1(t) + x_2(t) = k\cos(3t) + \cos(\sqrt{72}t), \qquad (1)$$

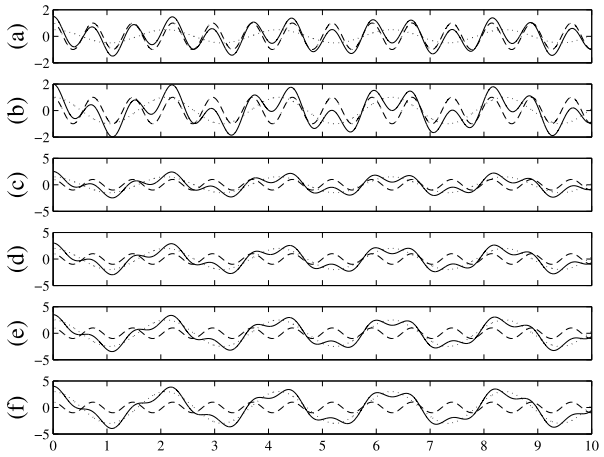

FIGURE 1. $x(t) = x_1(t) + x_2(t) = k\cos(3t + \phi_1) + \cos(\sqrt{72}t + \phi_2)$ is a quasi-periodic signal (the solid line). It includes two components $x_1(t)$ (the dot line) and $x_2(t)$ (the dot-dash line). $(a) \sim (f)$ corresponding to $k = 0.5, 1, 1.5, 2, 2.5, 3$, respectively.

which consists of two periodic components, where the constant k serves as the weight of signal $x_1(t)$. Obviously, the two components $x_1(t)$ and $x_2(t)$ have no common period, hence, $x(t)$ is a quasi-periodic signal. Fig.1 shows the signal $x(t)$ (the solid line), and its two components $x_1(t)$ (dot line) and $x_2(t)$ (dot-dash line) within the time interval [0, 10]. The curves of $x(t)$ in Figs. 1 (a) ~Figs. 1 (f) corresponding to $k = 0.5, 1, 1.5, 2, 2.5, 3$, respectively. From Fig.1 (a), we can see that $x(t)$ is not strictly periodic, but it looks like ''periodic'' to a large extent, and intuitively, its periodic behavior is mainly controlled by $x_2(t)$. In Fig.1 (b), the periodicity of $x(t)$ is obviously weaker than that in Fig.1 (a). The reason is that the two periodic components have almost equal energies. In other words, in this case, the signal does not have a dominant component. Figs.1$(c) \sim (f)$ show that the periodicities of $x(t)$ are gradually strengthened when k changes from 1.5 to 3, and the principal periodic behavior is more and more controlled by the component $x_1(t)$.

From the above example, one has no difficulty noticing such a fact that the degrees of periodicity are different for distinct quasi-periodic signals. Some of them have higher periodic degree, and even look like strict periodic signals, and some are not. After examining a number of examples, we realize that the periodic degree of a quasi-periodic signal depends on its constitution. If there exists a dominant period component in a quasi-periodic signal, it must show a certain degree of periodicity. Moreover, the greater the proportion of energy of the dominant period component to total energy of the signal is, the higher the degree of periodicity is. Based on the above observation and analysis, we define periodic degree(PD) and Dominant Period Component (DPC) as follows:

Definition 1: Suppose that $x(t) \in \mathbf{R}^T$ is a quasi-periodic signal consisting of N period components, written as $x(t) = \sum_{i=1}^{N} a_i x_i(t)$, where a_i represent the amplitude of ith period component $x_i(t)$ and $a_m = \max\{a_i, i = 1, 2, \cdots, N\}$.

The periodic degreeof $x(t)$, denoted by $PD(x)$, is defined as

$$PD(x) = \frac{a_m}{\sum_i a_i} \tag{2}$$

If a_m is the unique maximum of set $\{a_i, i = 1, 2, \cdots, N\}$, then $x_m(t)$ is defined as Dominant Period Component (DPC) of $x(t)$.

The main period behavior of a quasi-periodic signal is determined by its DPC, and its degree of periodicity is measured by PD. For example, let us compare the two quasi-periodic signals in Fig. 1 (a) and Fig. 1 (c), whose DPCs are $x_2(t)$ and $x_1(t)$, respectively. Due to their distinct DPCs, they exhibit different period behavior. While comparing Fig. 1 (c) and Fig. 1 (f), one has no difficulty seeing that because of having the same DPC, the two quasi-periodic signals show similar period behavior, but obviously different degrees of periodicity. According to the definition, their PDs are $1.5/2.5 = 0.6$ and $3/4 = 0.75$, respectively. The latter's PD is higher than that of the former, and intuitively, the latter looks more ''periodic'' than the former.

However, for a real quasi-periodic signal, it is usually hard to pick out the DPC and get the PD. Empirical Mode Decomposition (EMD) is a fully data-driven algorithm, with which, an arbitrary discrete signal $x(t) \in \mathbf{R}^T$ can be adaptively decomposed into a finite and often small number of IMFs and a residue, denoted by $x_i(t)(i = 1, \cdots, n)$ and $r(t)$ respectively, where T indicates the length of $x(t)$, and n is a nonnegative integer depending on the signal itself, i.e.,

$$x(t) = \sum_{i=1}^{n} x_i(t) + r(t). \tag{3}$$

EMD is indeed like sifting: to separate the local modes of a signal, from the finest scale component to the mean trend. The first IMF includes the finest scale component, namely the highest frequency component, and the residue is the mean trend which is the lowest frequency component or can also be viewed as the substitute of the DC term in Fourier expansion. Here we just take an example to show what will be obtained when EMD acts on a signal, the readers are referred to [25] for details. The first line of Fig. 2 is the noised signal $x(t) = 2\cos(3t) + \cos(\sqrt{72}t) + n(t)$, where $n(t)$ is an additive Gaussian white noise, Signal-Noise Ratio is set to $20dB$. By using EMD, it is decomposed into 10 IMFs and a residue, as shown in the rest rows of Fig. 2. We can see that the first 6 IMFs include the higher frequency components of the signal. They mainly come from the noise. The two main components which are $2\cos(3t)$ and $\cos(\sqrt{72}t)$ mainly are contained in the 7th and the 8th IMFs. The residue represents the lowest frequency trend.

IMFs may be seen as the substitutes of the signal's harmonic components, but because of having adaptivity, they are more natural than the harmonic components. An IMF is also treated as a monocomponent function, hence the instantaneous frequency can be reasonably defined, based on which the Hilbert spectral analysis is found. For the IMF, $x_i(t)$, its

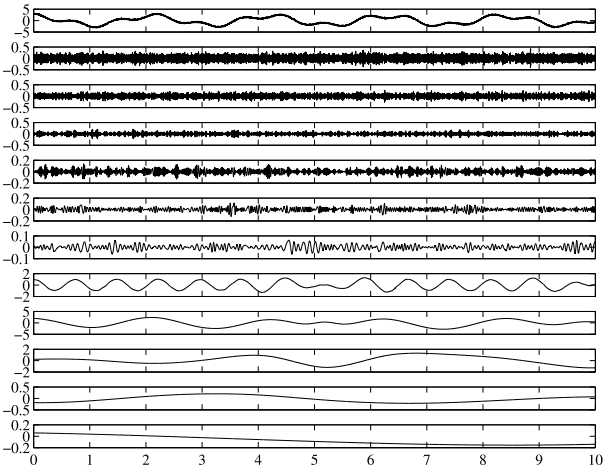

FIGURE 2. An example of EMD. The first line is the noised signal $x(t) = 2\cos(3t) + \cos(\sqrt{72}t) + n(t)$. The second line is the first IMF, and the rest lines, from top to bottom, successively are the second until to the 10th IMFs as well as the residue.

Hilbert transform $y_i(t)$ is defined by:

$$y_i(t) = \frac{1}{\pi} P \int_{-\infty}^{\infty} \frac{x_i(t')}{t - t'} dt', \tag{4}$$

where P indicates the Cauchy principal value. Consequently, $x_i(t)$ and $y_i(t)$ can form a complex conjugate pair, so that an analytic signal $z_i(t)$ can be produced:

$$z_i(t) = x_i(t) + jy_i(t) = a_i(t)e^{j\theta_i(t)}, \tag{5}$$

where

$$a_i(t) = \sqrt{x_i^2(t) + y_i^2(t)}, \quad \theta_i(t) = \arctan \frac{y_i(t)}{x_i(t)} \tag{6}$$

are the instantaneous amplitude and the phase, respectively. Further, the instantaneous frequency of $x_i(t)$ is defined as:

$$f_i(t) = \frac{d\theta_i(t)}{dt}. \tag{7}$$

According to Eqs. (5) and (7), $x_i(t)$ can be expressed as the real part, Re, in the following formula:

$$x_i(t) = Re\left[a_i(t) \exp\left(j \int f_i(t)dt\right)\right]. \tag{8}$$

Therefore, from Eqs. (3) and (8), $x(t)$ can be represented by

$$x(t) = \sum_{i=1}^{n} Re\left[a_i(t) \exp\left(j \int f_i(t)dt\right)\right] + r(t). \tag{9}$$

Eq. (9) enables us to represent the amplitude as a function of time(space) and instantaneous frequency, which can be defined mathematically as follows:

Definition 2: Let $x(t)$ be decomposed into finite Intrinsic Mode Functions (IMFs), $x_i(t)$ $(i = 1, \cdots, n)$ and a residue $r(t)$, then,

$$H(f, t) = \begin{cases} 0 & \text{if } J_{f,t} \text{ is an empty set,} \\ \sum_{i \in J_{f,t}} a_i(t), & \text{otherwise,} \end{cases} \tag{10}$$

where $J_{f,t} = \{i | 0 \le i \le n \text{ satisfying } f_i(t) = f\}$.

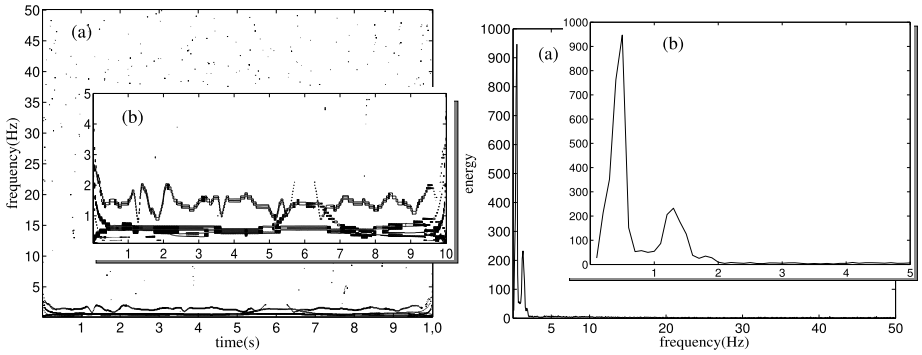

FIGURE 3. Left panel (a): Hilbert spectrum of the signal $x(t) = 2\cos(3t) + \cos(\sqrt{72}t) + n(t)$; Left panel (b): The local larger scale version of the low frequency band. Right panel (a): Marginal spectrum; Right panel (b): The local larger scale version of the low frequency band.

The time-frequency distribution of the amplitude is designated as the ''Hilbert amplitude spectrum'' or simply ''Hilbert spectrum'', denoted by $H(f, t)$. As an example, we show the Hilbert spectrum of the signal $x(t) = 2\cos(3t) + \cos(\sqrt{72}t) + n(t)$ on the left panel of Fig. 3. There are two evident high energy bands in the the Hilbert spectrum. They are apparently derived from $2\cos(3t)$ and $\cos(\sqrt{72}t)$ these two main components. In other words, the signal's main components have successfully been captured by the Hilbert spectrum.

Further, we integrate $H(f, t)$ along the time axis so that Hilbert marginal spectrum can be obtained, which is defined below:

Definition 3: The Hilbert marginal spectrum of $x(t)$ can be defined by

$$h(f) = \int_0^T H(f, t)dt. \tag{11}$$

The marginal spectrum is an energy distribution of a signal along with frequency axis. In other words, it is a measure of total energy contribution from each frequency value. As pointed out by Huang [25], the frequency in Hilbert spectrum or marginal spectrum has a totally different meaning from Fourier spectral analysis. In the Fourier representation, the existence of energy at a frequency means a component of sine or cosine wave persisted through the time (space) span of the data, while the existence of energy at the frequency means only there is a higher likelihood for such a wave to have appeared locally. That means even oscillations happen only in some locations, its frequency components still can be captured by Hilbert spectrum or marginal spectrum. Though it is difficult to theoretically prove this kind of energy distribution being superior to Fourier representation, a reasonable interpretation is that the adaptivity of EMD bate the so-called inter-harmonic components which are usually produced in Fourier decomposition. Therefore, a marginal spectrum represent signals's frequency structure more pertinent than a Fourier spectrum does.

The marginal spectrum of the signal mentioned above is shown on the right panel of Fig. 3. One has no difficulty seeing two peaks whose corresponding frequencies roughly equal to the ones of the two main components.

Before further discussion, we firstly give the definition of the main frequency of a quasi-periodic signal as follows:

Definition 4: Let $h(f)$ be the marginal spectrum of a quasi-periodic signal, the f_m is defined as the signal's Main Frequency (MF), if and only if

$$h(f_m) \geq h(f), \forall f \tag{12}$$

According to this definition, the MF is actually the frequency corresponding to the DPC. Therefore the PD can be computed as follows:

$$PD(x) = \frac{h(f_m)}{\int_f h(f)df} \tag{13}$$

where $\int_f h(f)df$ is the signal's total energy.

It should be pointed out that the whole EMD method was algorithmically proposed, which makes the strict theoretical analysis difficult. Hence, the next discussion is based on the hypothesis that the marginal spectrum of a signal obtained by [25] is an accurate representation of its energy distribution along with frequency axis, from which some properties of MF and PD can be concluded as follows:

Property 5: Both Main Frequency (MF) and periodic degree (PD) of a quasi-periodic signal are insensitive to changes of monotonic trend.

Proof: When EMD is applied to a signal with a monotonic trend, the IMFs will keep invariant except for the residue. According to the reference [25], a residue is similar to the DC in Fourier transform, and is not included in the computation of Hilbert spectrum. Consequently, both MF and PD of a quasi-periodic signal will also remain invariant when a monotonic trend is added to it.

Property 6: Main Frequency (MF) of a quasi-periodic signal are robust to an additive random white noise.

Proof: Theoretically, the energy of an additive random white noise will be distributed evenly on the entire frequency axis, then it just leads to a whole upper shift of marginal

spectrum instead of a change of the frequency at which the energy reaches the maximum.

Property 7: An additive random white noise will decreases periodic degree (PD) of a quasi-periodic signal.

Proof: Let W_f be the bandwidth of a quasi-periodic signal x, $\widehat{W}_f$ be that of an additive random white noise, and $\widehat{W}_f \geq W_f$. A is the intensity of noise. Then PD of the noisy quasi-periodic signal, denoted by x', can be written as follows:

$$P_d(x') = \frac{h(f_m) + A}{\int_f h(f)df + A\widehat{W}_f}. \tag{14}$$

Since $\widehat{W}_f \geq W_f$, we have

$$P_d(x') < \frac{h(f_m) + A}{\int_f h(f)df + AW_f}. \tag{15}$$

According to the integral mean value theorem, $\exists \xi$ satisfy

$$\int_f h(f)df = h(\xi)W_f. \tag{16}$$

Review Definition 12, we have $h(f_m) \geq h(\xi)$, hence

$$W_f = \frac{\int_f h(f)df}{h(\xi)} \geq \frac{\int_f h(f)df}{h(f_m)}. \tag{17}$$

Substituting Inequality 17 into Inequality 15, we can reach

$$\begin{aligned} P_d(x') &< \frac{h(f_m) + A}{\int_f h(f)df + AW_f} \\ &\leq \frac{h(f_m) + A}{\int_f h(f)df + A\frac{\int h(f)df}{h(f_m)}} \\ &= \frac{h(f_m)}{\int_f h(f)df} = P_d(x). \end{aligned} \tag{18}$$

As we know, the frequency controls a periodic signal's oscillation rate, and then is an important property of a periodic signal. For a quasi-periodic signal, its MF as well as PD also play a key role to control the signal's behavior, from the viewpoint of pattern recognition, which means that some unexpected results may be obtained if they are taken as classification features. This motivates us to propose the following method for texture features extracting.

III. TEXTURE FEATURES BASED ON THE MFS OF QUASI-PERIODIC SIGNALS

In this section, we will firstly introduce a kind of new texture feature based on the MFs of quasi-periodic signals, which is followed by an invariance discussion.

A. TEXTURE FEATURES BASED ON THE MFS OF QUASI-PERIODIC SIGNALS

As a special kind of image, texture images generally consist of some basic elements which are similar to each other and interlaced with each other, and exhibit obvious quasi-periodicity. Texture images are deemed to be typical quasi-periodic signals [21].

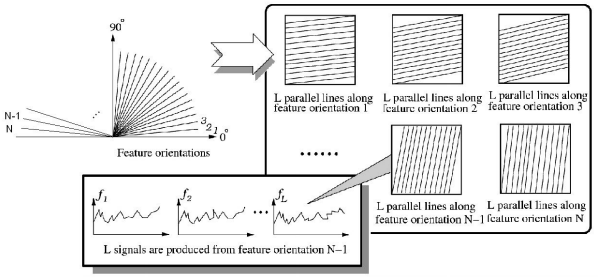

FIGURE 4. A sketch map of FOs. The top left: N equidistant FOs between 0° and 180°; The right: L equidistant lines along with each FO; The bottom left: L signals along with a FO.

However, we have to face a problem that the quasi-periodic signals discussed above are all one-dimensional signals, while the texture images are two-dimensional. It is really a tricky issue and at the moment we do not have a good solution yet. In this paper, we use a somewhat clumsy method that is sampling a texture image in some directions to produce one-dimensional signals. Since most texture images usually show different quasi-periodicity in different directions, we have to pick out one-dimensional signals in as many directions as possible to achieve an overall characterization of texture images. Obviously, the more the considered orientations are, the more overall the characterization the texture has, but the higher the computational complexity is. Without loss of generality, we set the 0° angle at horizontal direction, and select counterclockwise N equidistant angles between 0° and 180° as Feature Orientations (FOs) as follows:

$$D = \{d_i | d_i = (i-1)\frac{180}{N}, i = 1, 2, \cdots, N\}. \tag{19}$$

Practically, an appropriate N must be chosen to trade-off the accuracy and the computational complexity.

The complexity of texture images is also embodied in their randomness that there may exist differences between lines, even if they have the same orientation. To accurately extract the MF of each FO, we pick out L equidistant rows in each FO to form a quasi-periodic signal set, as shown in Fig. 4. Let x_{ij} be jth signal of ith FO, then the signal set of ith FO can be denoted as $X_i = \{x_{ij}, j = 1, \cdots, L\}$. For each $x_{ij} \in X_i$, computing its marginal spectrum h_{ij}, then the average marginal spectrum of the ith FO can be obtained

$$h_i(f) = \frac{\sum_{j=1}^{L} h_{ij}(f)}{L}, \tag{20}$$

based on which, we give the definition of Orientation Main Frequency (OMF) as follows:

Definition 8: Let $h_i(f)$ be the average marginal spectrum of a texture image in the ith feature orientation, the Orientation Main Frequency (OMF) of the ith feature orientation, denoted as omf_i, is defined as

$$omf_i = \arg\max_f \{h_i(f)\}. \tag{21}$$

Experiments show that an appropriate L is enough to make the determined OMF statistically reliable. From each FO, one can extract a unique OMF. The N OMFs corresponding to N FOs form a feature vector as follows:

$$\begin{aligned} V &= (v_1, v_2, , \cdots, v_N) \\ &= (omf_1, omf_2, \cdots, omf_N). \end{aligned} \tag{22}$$

On the other hand, for most texture images, the PDs at different orientations are distinct. To utilize this information, we similarly give the definition of Orientation Periodic Degree (OPD) as follows:

Definition 9: Let $h_i(f)$ and omf_i be the average marginal spectrum and the Orientation Main Frequency (OMF) in the ith feature orientation, respectively, the Orientation Periodic Degree (OPD) of the ith feature orientation is defined as

$$OPD_i = \frac{h_i(omf_i)}{\int_f h_i(f)df}. \tag{23}$$

Obviously, the orientations with higher PDs will play more important roles in texture classification than those with lower PDs. So it is a good idea to let them act as weights in each FO. To make these PDs a weight vector, we must normalize them as follows:

$$\widehat{OPD_i} = \frac{OPD_i}{\sum_i OPD_i}. \tag{24}$$

Then a weight vector is produced as follows:

$$\begin{aligned} W &= (w_1, w_2, , \cdots, w_N) \\ &= (\widehat{OPD}_1, \widehat{OPD}_2, \cdots, \widehat{OPD}_N) \end{aligned} \tag{25}$$

Combining equation (22) and equation (25), we give the final feature vector which consists of the weighted OMFs along with N FOs:

$$V_w = (w_1 v_1, w_2 v_2, , \cdots, w_N v_N) \tag{26}$$

We select three texture images as examples to view whether do the proposed features characterize the periodicity of texture images. They are D56, D35 and D37 in Brodatz album. These three textures have the following characteristics: D56 has obvious directionality, and its period in horizontal direction is obviously larger than that in vertical direction, while D36 and D37 have no obvious directionality; the period of D36 is smaller than that of D35. We randomly extract a sub-block with the size of 256×256 pixels from each texture image as shown on the top of Fig. 5. For each sub-block, let $N = 32, L = 40$, and compute OMFs and $\widehat{OPDs}$ as shown in the middle and bottom of Fig. 5, in which the legends $'\triangle'$, $'\circ'$, and $'\square'$ represent D56, D35 and D36, respectively. The middle of Fig. 5 shows that the OMFs along all FOs of D35 and D36 have hardly regular differences, while those of D56 monotonously increase from horizontal to vertical direction and reach the maximum, and then start to decrease monotonously. We also see that the marks $'\square'$ are always over those $'\circ'$, which means the OMFs along all FOs of D36 are larger than those of D35. The bottom of Fig. 5 shows that

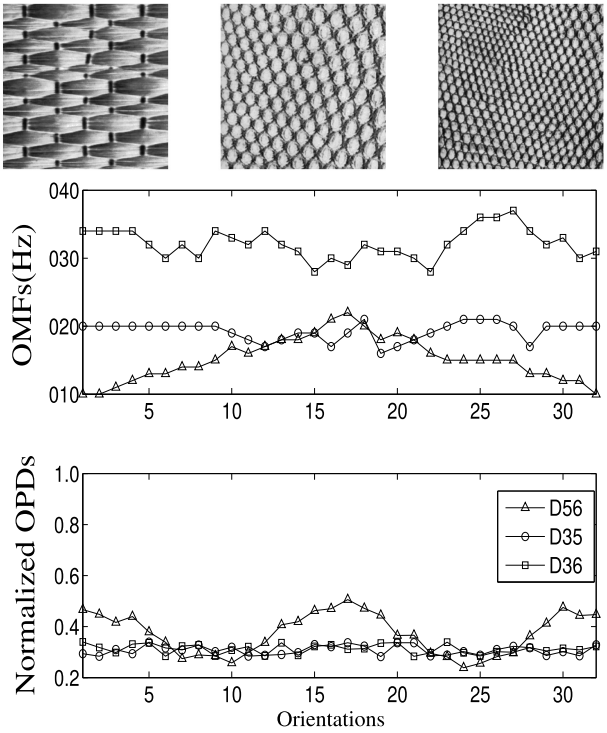

FIGURE 5. Top: Sub-blocks with the size of 256 × 256 from three kinds of texture images of the Brodatz album labeled by D56, D35 and D36; Middle: The OMFs of each sub-block along $N = 32$ FOs; Bottom: The $\widehat{OPDs}$ of each sub-block along each FO.

$\widehat{OPDs}$ along distinct FOs of D35 and D36 exhibit scarcely differences, while the $\widehat{OPDs}$ of D56 near the horizontal and vertical orientations are distinctly larger than those in other directions. These results are consistent with our visual perception, indicating that the proposed features can effectively capture the periodicity of texture images.

B. INVARIANT PROPERTIES

This section discusses invariance of the proposed features with regards to uneven illumination and rotation, as well as robustness to noise. The proposed features in Section III-A are based on the assumption that a signal which is extracted from a texture image along a FO is quasi-periodic. Hence, those properties discussed in Section II can be used to investigate invariant properties of the proposed features.

1) ILLUMINATION INVARIANT

A texture image is often contaminated by uneven illumination in many applications such as computer vision, remote sensing image analysis, scene analysis and so on. A texture classification feature with an invariant illumination is especially useful in these applications.

Firstly, we conduct an experiment to gain some experience on illumination invariance of the proposed features. Fig.6 (a) shows a sub-block with the size of 256×256 extracted from D56 of the Brodatz album, on which three kinds of uneven illuminations are exerted to compose three contaminated

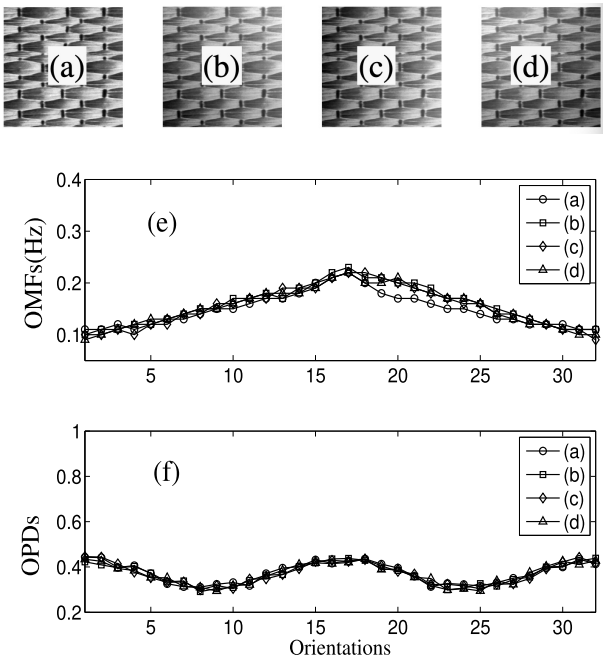

FIGURE 6. (*a*): A sub-block with the size of 256 × 256 extracted from D56 of the Brodatz album; (*b*) ∼ (*d*): Three contaminated versions; (*e*): The OMFs of three contaminated versions and the original version along selected FOs; (*f*): The $\widehat{OPDs}$ of four versions along all FOs.

versions as shown in Fig.6 (*b*) ∼ Fig.6 (*d*). Their OMFs and $\widehat{OPDs}$ along the selected FOs are plotted in Fig.6 (*e*) and Fig.6 (*f*), in which the symbols $'\circ', '\square', '\diamond'$ and $'\triangle'$ are used to mark the four versions shown in Fig.6 (*a*) ∼ Fig.6 (*d*), respectively. One has no difficulty seeing that both OMFs and $\widehat{OPDs}$ of the all four versions along each FO exhibit scarcely difference, which implies that the proposed features are really insensitive to uneven illuminations.

What brings such a good performance? Let x_{ij} be a signal extracted from a texture image, and $\widehat{x}_{ij}$ be the counterpart from some contaminated version. We notice that the difference between x_{ij} and $\widehat{x}_{ij}$ is just a monotonic trend to which both MF and PD of a quasi-periodic signal are insensitive according to Property 5 in Section II. Hence, the proposed features naturally have an excellent invariant property to uneven illumination.

2) ROTATION INVARIANT

The proposed features are the weighted OMFs along selected N FOs. They are obviously sensitive to any texture image's rotation. However, we notice that if the rotation angle of the texture image is just an integral multiple of $\frac{180^o}{N-1}$, then the rotation just leads the feature vector to left (or right) roll the same time. In other words, in this case, a rotation of a texture image is equivalent to a left (or right) roll of its feature vector.

Practically, the rotation angles often are not integral multiples of $\frac{180^o}{N-1}$. A deviation from a FO will bring an error of the weighted OMF along the FO, and the smaller the deviation

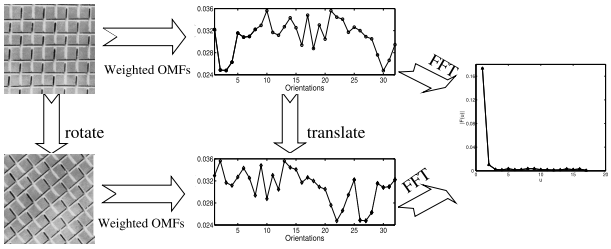

FIGURE 7. The sketch map of rotation invariant feature.

TABLE 1. Recognition rates of Dataset-1 (%).

Texture	D9	D10	D15	D17	D20	D22
Literature [10]	79	82	78	93	96	80
Literature [1]	78.75	83.75	67.75	93.75	98.75	92.5
Ours	92.5	100	100	100	100	100
Texture	D29	D37	D49	D51	D68	D77
Literature [10]	93	89	78	87	89	86
Literature [1]	67.5	58	77.5	78.75	82.5	93
Ours	92.5	100	100	97.5	100	100
Texture	D84	D93	D103	Aver.		
Literature [10]	81	79	79	84.6		
Literature [1]	61.25	88.75	92	81		
Ours	100	100	100	98.83		

TABLE 2. Error recognition rates of Dataset-1 (%).

Texture	D9	D29		D51
Mismatched as	D29	D9	D10	D29
Percentage	7.5	2.5	5	2.5

is, the smaller the error is. That means for a texture image and a rotation angle $\frac{180^o}{N-1}i < \alpha < \frac{180^o}{N-1}(i+1)$, if V_i and V_{i+1} are the feature vectors of the rotated versions with the angles of $\frac{180^o}{N-1}i$ and $\frac{180^o}{N-1}(i+1)$ respectively, then the feature vector V_α of the rotated version with the angle of α will be near V_i or V_{i+1}.

As well know, the energy spectrum of Fourier transform has good shift invariant property, hence, if V_{wf} is the energy spectrum of Fourier transform of the feature vector V_w, then V_{wf} will be insensitive to shifts of V_w, namely V_{wf} is approximately invariant to a rotation of texture images. Fig. 7 shows the sketch map of rotation invariant features. Considering the energy concentration property of the Fourier energy spectrum, we just pick out the first K items of V_{wf} to form the final feature vector which is approximately rotation invariant as follows:

$$V_{wf} = (v_{wf1}, v_{wf2}, \cdots, v_{wfK}). \tag{27}$$

3) ROBUSTNESS TO NOISE

According to Property 6 in Section II, an additive random white noise is insensitive to MF. The proposed features consist of weighted MFs of some quasi-periodic signals, hence they are robust against additive random white noises. But on the other hand, additive random white noises make the PD decreasing according to Property 7, the weights in feature vector will be contaminated and will cause its robustness to noise to weaken somewhat.

TABLE 3. Recognition rates of Dataset-2 (%).

Texture	D9	D23	D25	D27	D50	D53	D81	D84
PCC	87.5	85	97.5	92.5	97.5	97.5	95	85
Texture	D86	D92	D93	D105	D110	Others	Aver.	
PCC	97.5	82.5	97.5	90	92.5	100	98.29	

TABLE 4. Error recognition rates of Dataset-2 (%).

Texture	D1	D5	D9		D18	D23	D25	
Mismatched as	D105	D86	D4	D81	D56	D27	D37	D105
Percentage	2.5	2.5	10	2.5	2.5	20	2.5	5
Texture	D27	D50	D53	D81		D84	D86	D92
Mismatched as	D23	D25	D77	D10	D56	D4	D66	D10
Percentage	7.5	10	10	5	5	15	2.5	25
Texture	D93	D105		D110				
Mismatched as	D78	D47	D9	D10	D84			
Percentage	2.5	15	2.5	2.5	2.5			

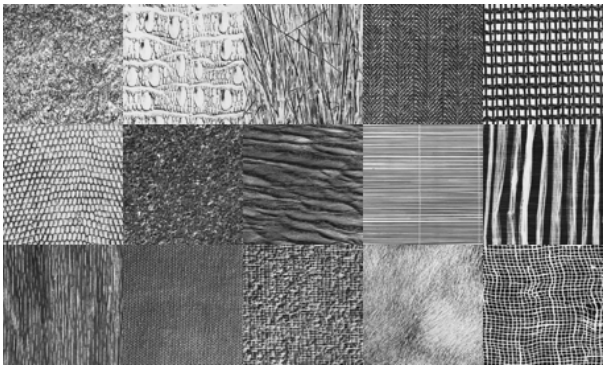

FIGURE 8. Texture samples from Dataset-1 (from left to right): First row — D9, D10, D15, D17, D20; Second row — D22, D29, D37, D69, D51; Third row— D68, D77, D84, D93, D103.

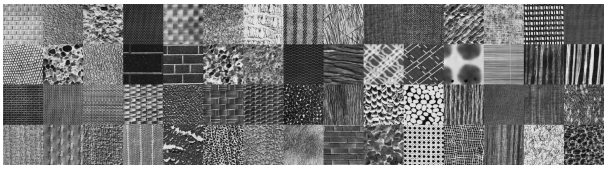

FIGURE 9. Texture samples from Dataset-2 (from left to right): the 1st row: D1, D4, D5, D6, D8,D9, D10, D11, D15, D16, D17 D18, D19, D20, D21; the 2nd row: D22, D23, D24, D25, D26, D27, D28, D34, D37, D46, D47, D48, D49, D50, D51; the 3rd row: D52, D53, D55, D56, D57, D64, D65, D66, D68, D74, D75, D76, D77, D78, D81; the 4th row: D82, D83, D84, D85, D86, D87, D92, D93, D94, D98, D101, D103, D105, D110, D111.

IV. EXPERIMENTAL RESULTS AND ANALYSIS

Three data sets of texture images will be employed in the experiments to demonstrate the performance of the proposed features. Dataset-1 consists of 15 kinds of texture image from Brodatz album. They were also used in the experiments of [1], [10]. Some samples are shown in Fig. 8.

Dataset-2 consists of 60 texture images, as shown in Fig. 9, that were experimented in [11]. Dataset-3 contains 30 textures, as shown in Fig. 10, which were used in [6]–[9].

In the experiments, the texture images are converted into the gray-scale versions. In the training phase, 5 sub-images

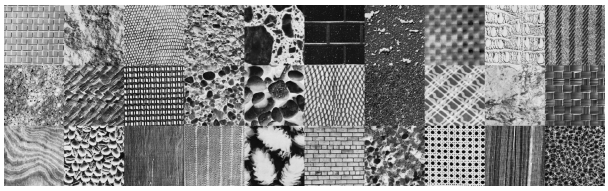

FIGURE 10. Dataset-3: D1, D2, D22, D5, D62, D25, D86, D8, D10, D11, D73, D18, D20, D23, D31, D35, D29, D46, D63, D64,D71, D74, D79, D85, D88, D95, D27, D101, D105, and D111 from left to right and top to bottom.

TABLE 5. The average classification rates of different methods for Dataset-3 (%).

Ref. [7]	Ref. [6]	Ref. [8]	Ref. [9]	Ours
85.23	87.25	91.56	96.28	98.42

of size 256 × 256 pixels are extracted randomly from each class of texture images, and denote jth sample of ith class as $T^{i,j}(j = 1, 2, \cdots, 5)$ for simplicity. For each extracted sub-image, set the 0° angle at the horizontal direction, and select counterclockwise $N = 32$ equidistant angles between 0° and 180° as FOs. From each FO, pick out $L = 40$ equidistant rows to form the signal set $X_i(i = 1, 2, \cdots, L)$. Then compute the final feature vector of each sub-images according to Section III. The minimum distance classifier is employed to determine an unknown sample's classification.

The detailed results on Dataset-1 are illustrated in Table 1. For the sake of comparison, the results in literature [1], [10] are reported in the same table. We can see that the results based on the proposed features are much better than those of literature [1], [10].

The confusion maps are illustrated in Table 2, in which the first row contains the actual textures, the next two rows represent the mismatched classes and their percentages of the confusion maps respectively. For example, the percentages of D29 mismatching to D9 and D10 are 2.5% and 5%, respectively.

TABLE 6. Recognition correct rates for uneven illuminations (%).

Texture	D9	D10	D15	D17	D20	D22	D29	D37
LF	95	95	100	100	100	100	90	100
GF	95	100	100	100	100	95	95	100
Texture	D49	D51	D68	D77	D84	D93	D103	Aver.
LF	100	95	100	100	95	100	100	98
GF	100	100	100	100	90	100	100	98.33

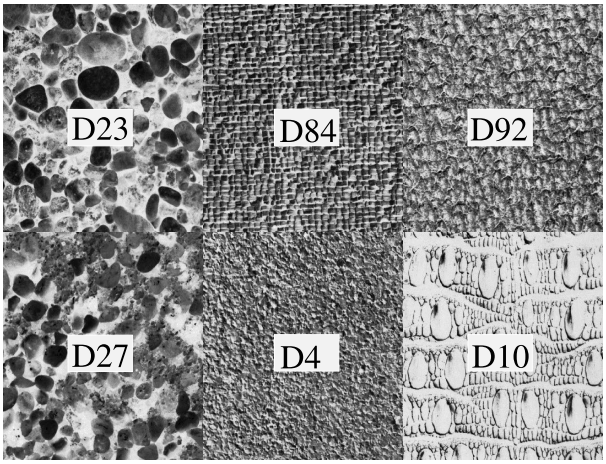

FIGURE 11. Three most confusing pairs of textures, where the two texture images of each column is a pair.

The method of reference [10] only selects the samples of rotation 20°, 70°, 90°, 120° or 150° to train, thus, in the test phase, the test samples must also be rotated at these angles. Our method only needs the original sample in the training phase, whereas the test sample can rotate any angle.

When the experiments are conducted on Dataset-2, 47 of 60 classes of textures which are D1, D4, D5, D6, D8, D10, D11, D15, D16, D17, D18, D19, D20, D21, D22, D24, D26, D28, D34, D37, D46, D47, D48, D49, D51, D52, D55, D56, D57, D64, D65, D66, D68, D74, D75, D76, D77, D78, D82, D83, D85, D87, D92, D94, D98, D101, D103 and D111 achieve a recognition rate of 100%. The percentage of correct classification of other classes are shown in Table 3, in which the percentage of correct classification is denoted as "PCC" for simplicity. We have observed that the worst is 82.5% and the average rate is 98.29%, which is better than the best rate 96.7% in [11]. Similarly, Table 4 shows the confusion map.

Fig. 11 shows the three most confusing pairs of textures. Intuitively, they indeed have great similarities.

We also tested the proposed feature on Dataset-3. The experimental results are shown in Table 5. For the sake of simplicity, we only list the average classification rates. It shows that the average classification accuracy of our method is as high as 98.42%, which far exceeds the results of literature [6]–[8], slightly better than that of literature [9].

To evaluate the performance of the proposed features to uneven illumination, we test 16 kinds of uneven illuminations as shown in Fig. 12. They are produced by mathematical

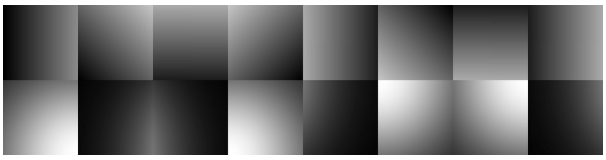

FIGURE 12. Sixteen kinds of uneven illumination (from top to bottom): First row — 2D linear function; Second row — 2D Gaussian function.

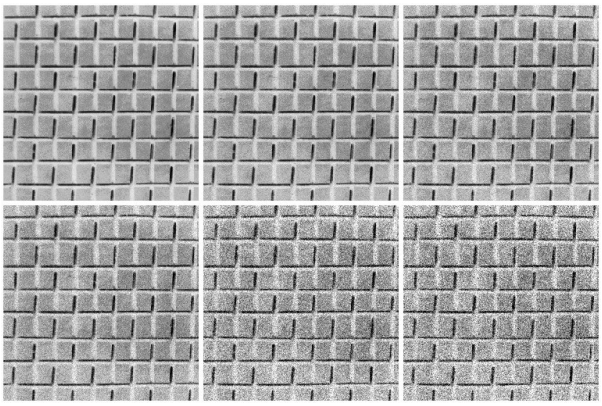

FIGURE 13. Noisy texture samples with different SNR levels (from left to right): First row— original texture, $SNR = 30dB$, $SNR = 20dB$; Second row— $SNR = 15dB$, $SNR = 10dB$, $SNR = 5dB$.

TABLE 7. Recognition correct rates under different noise levels (%).

SNR (dB)	30	20	15	10	5
PCC	97.33	94.67	93.33	87	80.33

functions, which are divided into two groups: (1) 2D linear function (see First row of Fig. 12), and (2) 2D Gaussian function (see Second row of Fig. 12). Dataset-1 is employed again. Forty samples of size 256×256 pixels are extracted from each class of texture images, twenty of which are added randomly to the linear uneven illuminations and the other 20 samples are added randomly to the Gaussian uneven illuminations. The recognition results are shown in Table 6, in which "LFs" and "GFs" express linear function and Gaussian function, respectively. It is clear that only a slight drop in percentage of correct classification occurred when an uneven illumination is added to a testing sample, which can indicate that the proposed features really have an excellent invariance to uneven illuminations.

The final experiment is conducted to evaluate the robustness to white noise, where Dataset-1 is used again. One hundred samples of size 256×256 pixels are extracted from each class of textures, which are divided into 5 groups (20 samples

for each group). The Gaussian white noise, whose signal to noise ratios (SNR) are 30dB, 20dB, 15dB, 10dB and 5dB, are added to the samples in the different groups. Some samples with different SNR noises are shown in Fig. 13. Encouraging results have been achieved as shown in Table 7.

V. CONCLUDING REMARKS

This paper presents some new insights into quasi-periodic signals by introducing novel concepts on DPC (Dominant Period Component), PD (Periodic Degree), and MF (Main Frequency). They form the basis of our new method of extracting the key features from a real-life quasi-periodic signals i.e. the MF by using the Hilbert-Huang transform. For a quasi-periodic signal, MF is essentially the frequency of DPC. It controls the oscillation rate of a quasi-periodic signal and plays a key role in controlling the behavior of the entire signal. Hence, a good performance will be worth expecting if it serves as a classification feature. This is the main motivation of this paper.

Based on the above idea, a new texture feature which consists of the weighted Orientation Main Frequencies (OMF's) has been derived. Experiments confirm these salient properties of MF have generated a very high classification rates. Three data sets of texture images have been employed to evaluate the performance of the proposed features. Encouraging experimental results have been achieved.

In addition, the features are also invariant to uneven illumination, rotation, and are robust against noise. We have proved both MF and PD of a quasi-periodic signal are insensitive. Hence, the proposed features essentially have an excellent invariance to uneven illumination. This has also been verified by experimental results. Because the final feature vector consists of the energy spectrum of Fourier transform, the performance of rotation invariance only depends on the number of FOs (Feature Orientations). All experimental results listed above have been achieved under the condition that the number of FOs is 32. In fact, when the number of FOs is 16 or even smaller, the results are still better. Limited by space, the details have been left out in this paper. The proposed features consist of weighted MFs, we have demonstrated MFs of a quasi-periodic signal are robust to additive random white noises, but an additive random white noise decreases the PD. Hence, the proposed features have a better, but not perfect robustness to additive random white noises.

Finally, we have to point out that the rotation invariance of the proposed features is imperfect, and the way of obtaining rotation invariance seems somewhat clumsy. In future research, we will try new sampling ways to make up for this defect.

REFERENCES

[1] P. Campisi, S. Colonnese, G. Panci, and G. Scarano, "Reduced complexity rotation invariant texture classification using a blind deconvolution approach," *IEEE Trans. Pattern Anal. Mach. Intell.*, vol. 28, no. 1, pp. 145–149, Jan. 2006.

[2] A. Fernández, O. Ghita, E. González, F. Bianconi, and P. F. Whelan, "Evaluation of robustness against rotation of LBP, CCR and ILBP features in granite texture classification," *Mach. Vis. Appl.*, vol. 22, no. 6, pp. 913–926, Nov. 2011.

[3] S. Hegenbart and A. Uhl, "An orientation-adaptive extension to scale-adaptive local binary pattern," in *Proc. 22nd Int. Conf. Pattern Recognit.*, Stockholm, Sweden, Aug. 2014, pp. 1–6.

[4] P. Yang and G. Yang, "Feature extraction using dual-tree complex wavelet transform and gray level co-occurrence matrix," *Neurocomputing*, vol. 197, pp. 212–220, Jul. 2016.

[5] E. Jebamalar Leavline and D. Asir Antony Gnana Singh, "Local binary pattern family descriptors for texture classification," *I. J. Image, Graph. Signal Process.*, vol. 29, no. 4, pp. 439–448, Sep. 2011.

[6] G. H. Liu, L. Zhang, Y. K. Hou, Z. Y. Li, and J. Y. Yang, "Image retrieval based on multi-texton histogram," *Pattern Recognit.*, vol. 43, pp. 2380–2389, Jul. 2010.

[7] Z. Guo, L. Zhang, and D. Zhang, "A completed modeling of local binary pattern operator for texture classification," *IEEE Trans. Image Process.*, vol. 19, no. 6, pp. 1657–1663, Jun. 2010.

[8] Y. S. Kumari, V. V. Kumar, and C. Satyanarayana, "Texture classification using complete texton matrix," *Int. J. Image, Graph. Signal Process.*, vol. 9, no. 10, pp. 60–68, Oct. 2017.

[9] Y. S. Kumari, V. V. Kumar, and C. Satyanarayana, "Classification of textures based on noise resistant fundamental units of complete texton matrix," *Int. J. Image, Graph. Signal Process.*, vol. 10, no. 2, pp. 43–51, 2018.

[10] P. Campisi, A. Neri, G. Panci, and G. Scarano, "Robust rotation-invariant texture classification using a model based approach," *IEEE Trans. Image Process.*, vol. 13, no. 6, pp. 782–791, Jun. 2004.

[11] K. Jafari-Khouzani and H. Soltanian-Zadeh, "Radon transform orientation estimation for rotation invariant texture analysis," *IEEE Trans. Pattern Anal. Mach. Intell.*, vol. 27, no. 6, pp. 1004–1008, Jun. 2005.

[12] F. Riaz, A. Hassan, S. Rehman, and U. Qamar, "Texture classification using rotation-and scale-invariant Gabor texture features," *IEEE Signal Process. Lett.*, vol. 20, no. 6, pp. 607–610, Apr. 2013.

[13] Z. Li, G. Liu, Y. Yang, and J. You, "Scale- and rotation-invariant local binary pattern using scale-adaptive texton and subuniform-based circular shift," *IEEE Trans. Image Process.*, vol. 21, no. 4, pp. 2130–2140, Apr. 2012.

[14] S. Hegenbart and A. Uhl, "A scale- and orientation-adaptive extension of Local Binary Patterns for texture classification," *Pattern Recognit.*, vol. 48, no. 8, pp. 2633–2644, Aug. 2015.

[15] Z. Yang, Q. Zhang, F. Zhou, and L. Yang, "Hilbert spectrum analysis of piecewise stationary signals and its application to texture classification," *Digit. Signal Process.*, vol. 82, pp. 1–10, Nov. 2018.

[16] G. Tang, Z. Liu, and J. Xiong, "Distinctive image features from illumination and scale invariant keypoints," *Multimedia Tools Appl.*, vol. 78, no. 16, pp. 23415–23442, Aug. 2019, doi: 10.1007/s11042-019-7566-8.

[17] S. M. Tabatabaei and A. Chalechale, "Noise-tolerant texture feature extraction through directional thresholded local binary pattern," *Vis. Comput.*, to be published, doi: 10.1007/s00371-019-01704-8.

[18] Z. Liu, Z. Lai, W. Ou, K. Zhang, and R. Zheng, "Structured optimal graph based sparse feature extraction for semi-supervised learning," *Signal Process.*, vol. 170, May 2020, Art. no. 107456, doi: 10.1016/j.sigpro.2020.107456.

[19] L. Zhang, Q. Zhang, B. Du, X. Huang, Y. Y. Tang, and D. Tao, "Simultaneous spectral-spatial feature selection and extraction for hyperspectral images," *IEEE Trans. Cybern.*, vol. 48, no. 1, pp. 16–28, Jan. 2018.

[20] H. Bohr, *Fastperiodische Funktionen, Erg. Math*. Berlin, Germany: Springer, 1932.

[21] L. F. Chaparro and G. Shufelt, "Rational models for quasi-periodic signals," *Proc. IEEE*, vol. 74, no. 4, pp. 611–613, Apr. 1986.

[22] K. Nishi, "Kalman filter analysis for quasi-periodic signals," in *Proc. IEEE Int. Conf. Acoust., Speech, Signal Process.*, Salt Lake City, UT, USA, May 2001, pp. 3937–3940.

[23] J. Lim, A. Oppenheim, and L. Braida, "Evaluation of an adaptive comb filtering method for enhancing speech degraded by white noise addition," *IEEE Trans. Acoust., Speech, Signal Process.*, vol. ASSP-26, no. 4, pp. 354–358, Aug. 1978.

[24] R. Bitmead, A. Tsoi, and P. Parker, "A Kalman filtering approach to short-time Fourier analysis," *IEEE Trans. Acoust., Speech, Signal Process.*, vol. 34, no. 6, pp. 1493–1501, Dec. 1986.

[25] N. E. Huang, Z. Shen, S. R. Long, M. C. Wu, H. H. Shih, Q. Zheng, N.-C. Yen, C. C. Tung, and H. H. Liu, "The empirical mode decomposition and the Hilbert spectrum for nonlinear and non-stationary time series analysis," *Proc. Roy. Soc. London A, Math., Phys. Eng. Sci.*, vol. 454, no. 1971, pp. 903–995, Mar. 1998.
[26] P. Flandrin, G. Rilling, and P. Goncalves, "Empirical mode decomposition as a filter bank," *IEEE Signal Process. Lett.*, vol. 11, no. 2, pp. 112–114, Feb. 2004.

ZHIHUA YANG was born in Hunan, China, in 1964. He received the M.S. degree in automation from Hunan University, Changsha, China, in 1995, and the Ph.D. degree in computer science from Sun Yat-sen University, Guangzhou, China, in 2005.

He was a Visiting Scholar with the Center of Pattern Recognition and Machine Intelligence, Concordia University, Montreal, QC, Canada, in 2009. Since 2009, he has been a Professor with the Information Science School, Guangdong Finance and Economics University, Guangzhou. He has authored over 40 articles. His current research interests include signal analysis, pattern recognition, and image processing.

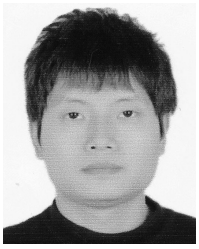

QIAN ZHANG received the B.S. degree in mathematics from Hunan University, China, in 2007, and the Ph.D. degree in science from Sun Yat-sen University and the City University of Hong Kong, in 2012. He participated in the cooperative training project between Sun Yat-sen University and the City University of Hong Kong, from 2007 to 2012. Since 2012, he has been an Assistant Professor with the College of Mathematics and Statistics, Shenzhen University, China. His current research interests include signal analysis and pattern recognition.

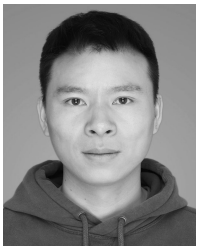

FENG ZHOU received the B.S. degree in information computing science from Minnan Normal University, China, in 2006, and the Ph.D. degree in computational mathematics from Sun Yat-sen University, China, in 2015. As a Visiting Student, he studied at the School of Mathematics, Georgia Institute of Technology, from September 2013 to September 2014. He is currently an Assistant Professor with the School of Information, Guangdong University of Finance and Economics. His research interests include signal analysis, machine learning, and ensemble learning.